Laser-capture microdissection for spatial transcriptomics of immunohistochemically detected neurons

Received for publication, September 22, 2024, and in revised form, November 29, 2024 Published, Papers in Press, December 28, 2024,
https://doi.org/10.1016/j.jbc.2024.108150

Balázs Göcz[1,*,‡], Éva Rumpler[1,*,‡], Soma Szentkirályi-Tóth[1], Katalin Skrapits[1], Szabolcs Takács[1], Miklós Sárvári[1], Imre Farkas[1], Szilárd Póliska[2], and Erik Hrabovszky[1,*]

From the [1]Laboratory of Reproductive Neurobiology, HUN-REN Institute of Experimental Medicine, Budapest, Hungary; [2]Department of Biochemistry and Molecular Biology, Faculty of Medicine, University of Debrecen, Debrecen, Hungary

Reviewed by members of the JBC Editorial Board. Edited by Kirill Martemyanov

We developed a versatile 'IHC/LCM-Seq' method for spatial transcriptomics of immunohistochemically detected neurons collected with laser-capture microdissection (LCM). IHC/LCM-Seq uses aluminon and polyvinyl sulfonic acid for inventive RNA-preserving strategies to maintain RNA integrity in free-floating sections of 4% formaldehyde-fixed brains. To validate IHC/LCM-Seq, we first immunostained and harvested striatal cholinergic interneurons with LCM. RNA preparations were subjected to random primer-based cDNA library preparation and bulk sequencing on the NextSeq Illumina platform. IHC/LCM-Seq detected ∼16,000 transcripts, reaching the sensitivity of a reference 'LCM-Seq method' developed for fluorescently tagged neurons microdissected from lightly formaldehyde-fixed and slide-mounted brain sections of transgenic mice. We successfully used the new IHC/LCM-Seq approach to provide unprecedented insight into the transcriptome of immunohistochemically detected gonadotropin-releasing hormone (GnRH) neurons regulating reproduction. The ∼13,000 to 14,000 transcripts identified in GnRH neurons of adult male rats and mice encoded 28 proteins implicated previously in human infertility, 35 neuropeptides, 34 nuclear receptors, and 164 G protein–coupled receptors. Functional experiments using slice electrophysiology established that the heavy *Ntsr2* expression conveys a strong excitatory action of neurotensin on GnRH neurons. As an unexpected species difference, we found that GnRH neurons exclusively expressed estrogen receptor-β in rats and against the current consensus, the alpha estrogen receptor isoform in mice. The IHC/LCM-Seq technique we are reporting is a highly sensitive and accurate bulk sequencing approach to characterize the transcriptome landscape of immunohistochemically labeled neurons, including neuroendocrine GnRH cells. This method is readily applicable to any species, opening new perspectives also for future studies of the *post mortem* human brain.

Gonadotropin-releasing hormone (GnRH) neurons form the final output pathway for the hypothalamic control of reproduction. Their processes projecting from the preoptic area to the external zone of the median eminence (1) release GnRH decapeptide into the hypophysial portal circulation. Upon binding to GnRH receptors in the adenohypophysis, GnRH stimulates the secretion of luteinizing hormone and follicle stimulating hormone which, in turn, act in the gonads to promote gametogenesis and sex steroid hormone production (2). Development of new methodological approaches to uncover the transcriptome landscape of GnRH neurons will be key to understanding the neuroendocrine regulation of the reproductive axis.

The earliest technical efforts to gain insight into the gene expression profile of GnRH neurons applied low-throughput and low-sensitivity methods, including single-cell RT-PCR (3) and dual-label *in situ* hybridization (4). High-throughput molecular techniques introduced later, such as microarray analysis of cytoplasmic samples collected with patch electrodes (5), laser-capture microdissection (LCM) of fluorescently tagged GnRH neurons coupled with microarray analysis (6), and ribosome affinity purification coupled with next-generation sequencing of RNA (RNA-Seq) (7), provided more complete information about the transcriptome landscape of murine GnRH neurons. Each of these approaches used earlier have unique advantages as well as limitations. Hybridization-based microarray technologies are increasingly replaced by methods using high throughput RNA-Seq which provides better dynamic range, higher reproducibility, and increased accuracy in differential expression analysis of both high- and low-abundance transcripts (8, 9). Recently, our laboratory has developed and reported in this journal an 'LCM-Seq' method to study fluorescently tagged neurons microdissected from lightly formaldehyde-fixed and slide-mounted brain sections of transgenic mice (10). This method also opened the way for a detailed transcriptome profiling of LCM-isolated murine cell types.

LCM-Seq (10) and other high-throughput methods rely on the use of genetically modified mouse models. Therefore, comprehensive information on the GnRH neuron transcriptome is entirely unavailable from other species. More in general, methodologies for transcriptome profiling of spatially and neurochemically defined neuron populations broadly usable in any species is still an unmet need. With this limitation

‡ These authors contributed equally to this work.
* For correspondence: Balázs Göcz, gocz.balazs@koki.hun-ren.hu; Éva Rumpler, rumpler.eva@koki.hun-ren.hu; Erik Hrabovszky, hrabovszky.erik@koki.hun-ren.hu.

in mind, the major goal of our study was to develop, validate, and use a versatile 'IHC/LCM-Seq' method to characterize the gene expression profile of neurons visualized in tissue sections with immunohistochemistry (IHC). Second, we aimed to use this newly developed IHC/LCM-Seq approach to provide unprecedented insight into the transcriptome landscape of GnRH neurons isolated from male rats and mice.

We set out to achieve the following goals: (i) IHC/LCM-Seq should be compatible with the use of 4% paraformaldehyde (PFA) fixative which is optimal for the IHC detection of peptidergic neurons. (ii) Long-term section storage should allow temporal separation of tissue collection from histological and molecular processing. (iii) Tissue RNA protection during IHC should not compromise the detection of various neuronal phenotype markers. (iv) The sensitivity and accuracy of the sequencing should be similar to those of a reference LCM-Seq technique we developed and validated recently on transgenic mice engineered to express the ZsGreen fluorescent marker protein selectively in cholinergic neurons (10). (v) Finally, IHC/LCM-Seq should allow us to characterize and compare the transcriptome profiles of rat and mouse GnRH neurons.

Results

Aluminon (0.05%, m/V) and polyvinyl sulfonate (PVSA; 2%, V/V) efficiently preserve RNA integrity during long-term storage of free-floating tissue sections in cryoprotectant

To separate the phases of tissue collection, IHC processing, LCM, and subsequent molecular procedures, our first goal was to solve the long-term storage of 4% PFA-fixed tissue sections without compromising RNA integrity. Lower fixative concentrations or alcohol-based 'molecular' fixatives that are unable to maintain the integrity of free-floating sections were not considered during method development. The aqueous cryoprotectant solution known to preserve peptide antigenicity for IHC (11) and mRNA integrity for *in situ* hybridization experiments (12) was supplemented with the potent RNase inhibitors aluminon (triammonium salt of aurintricarboxylic acid; 0.05%, m/V) (13) or 2% PVSA (V/V) (14) and used as a medium for −20 °C storage of 20-μm-thick free-floating sections of brains (N = 3) perfusion-fixed with 4% PFA. Three years later, total RNA was isolated from the archived sections with the PureLink FFPE kit for quality assessment with an Agilent 2100 Bioanalyzer system (Fig. 1*A*). RNA integrity number (RIN) was 3.0 ± 0.1 without using RNase inhibition, whereas either 0.05% aluminon (13) or 2% PVSA (14) efficiently protected the RNA against degradation (Fig. 1*A*; $RIN_{aluminon}$: 6.6 ± 0.1; RIN_{PVSA}: 7.1 ± 0.2). One-way ANOVA results (p = 5.89E-06; F = 163.083) followed by Tukey's *post hoc* test confirmed significantly higher RIN values in sections stored in the presence of aluminon ($p < 0.0001$) and PVSA ($p < 0.0001$) *versus* the RIN values of the unprotected sections. In further efforts to develop the IHC/LCM-Seq method, we preferentially used 0.05% aluminon to archive the sections because PVSA tended to cause clumping of the stored tissues.

0.05% aluminon or 2% PVSA in IHC reagents and wash buffers efficiently prevents RNA degradation

In a previous LCM-Seq study we used here as a reference method (10), we found that the RIN value of ∼5.5 was compatible with random primer-based library preparation and bulk sequencing protocols. As we were able to reach and even exceed this quality measure in sections stored in modified cryoprotectant solutions, we proceeded by testing to what extent various concentrations of aluminon and/or PVSA maintain the integrity of tissue RNA during IHC processing. Test brains (N = 3) were perfusion-fixed and postfixed for 5 h with ice-cold 4% PFA and infiltrated overnight at 4 °C with sterile 20% sucrose solution prepared in 0.1 M PBS (PBS; pH 7.6). Then, 20-μm-thick test sections were prepared with a cryostat for RNA isolation and quality assessments before and after IHC processing. Incubation in guinea pig anti-GnRH primary antibodies (#1018; 1:30,000) (15) was carried out at 4 °C for 35 h and subsequent steps (4 h; Fig. 1*B*) at room temperature. The pre-IHC RIN value of 8.3 ± 0.3 in this experiment fell to 2.9 ± 0.2 without inhibiting RNases. While the use of 0.0005% or 0.005% aluminon and 1% PVSA was entirely inefficient in preventing RNA degradation, the post-IHC RIN value was compromised only minimally when either 0.05% aluminon ($RIN_{aluminon}$: 6.6 ± 0.4) or 2% PVSA (RIN_{PVSA}: 7.0 ± 0.2) was included in buffers and antibody solutions, except for the peroxidase developer (Fig. 1*B*). One-way ANOVA (p = 1.51E-14; F = 103.943) followed by Tukey's *post hoc* tests confirmed that the post-IHC RIN values were significantly higher in sections processed in the presence of 0.05% aluminon ($p < 0.0001$) or 2% PVSA ($p < 0.0001$) in comparison with the RIN values of unprotected Ctrl sections.

While 2% PVSA does not affect the detection of various antigens, 0.05% aluminon can compromise the IHC results

We next tested if 0.05% aluminon or 2% PVSA interfere with the IHC detection of a series of neurotransmitter marker enzymes (choline acetyltransferase /ChAT/ and tyrosine hydroxylase /TH/) and neuropeptides (GnRH; proopiomelanocortin /POMC/ and orexin B /OXB/) (Fig. 1*C*).

While addition of 0.05% aluminon to the antibody and buffer solutions did not hinder the detection of GnRH neurons, it caused enhanced background staining, nonspecific labeling of cell nuclei, and reduced signal intensity when visualizing ChAT, TH, POMC, and OXB neurons (Fig. 1*C*). In contrast, all of these signals were preserved and artifacts were avoided using 2% PVSA for RNA protection (Fig. 1*C*).

Sensitivity and accuracy of the IHC/LCM-Seq method can be assessed from a reference transcriptome obtained via LCM-Seq studies of ZsGreen-tagged dorsal striatal cholinergic interneurons

Recently, we have reported in this journal a versatile 'LCM-Seq' methodology for deep transcriptome profiling of fluorescently tagged and spatially defined cholinergic neuron populations isolated with LCM from histological sections of

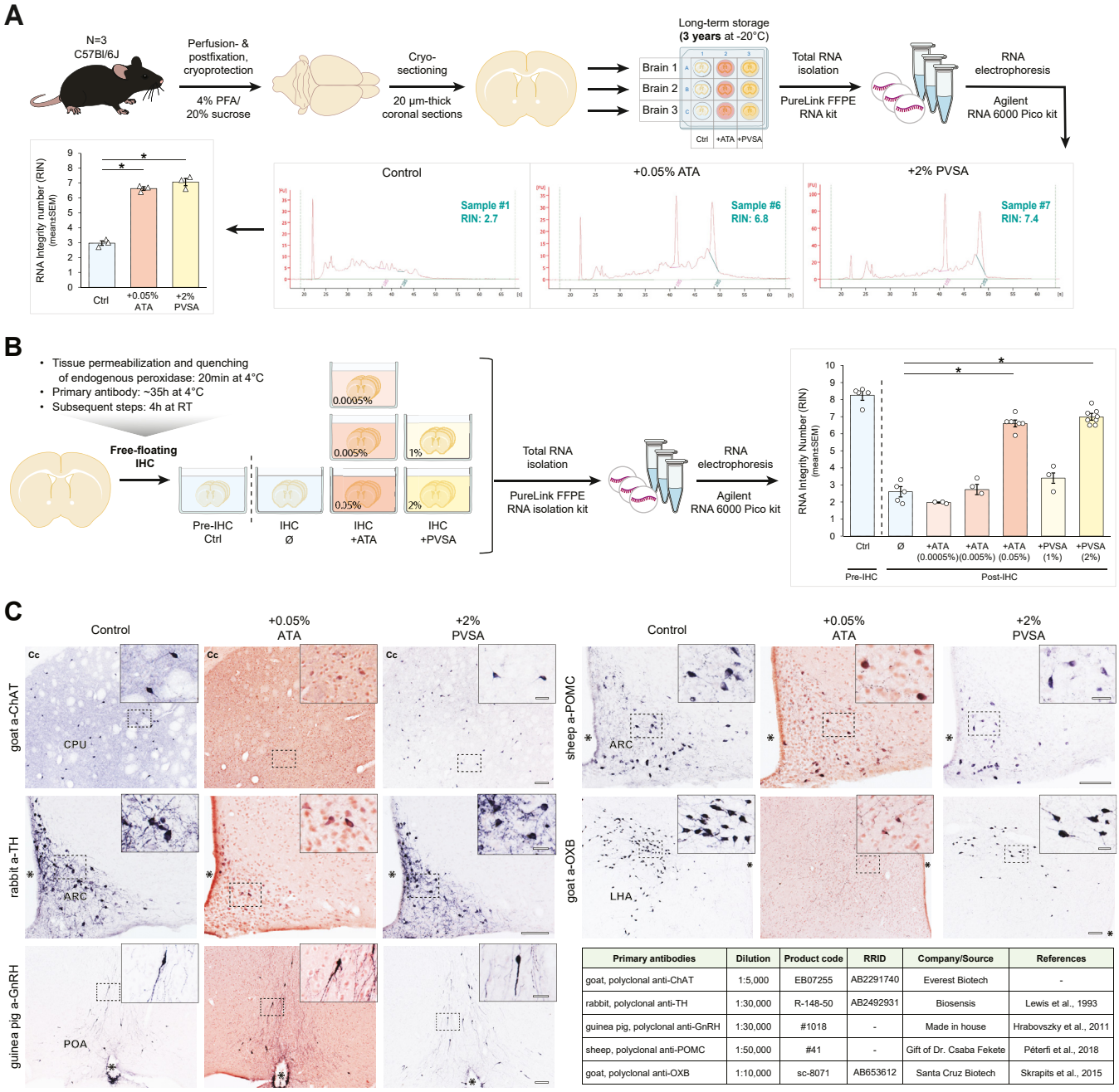

Primary antibodies	Dilution	Product code	RRID	Company/Source	References
goat, polyclonal anti-ChAT	1:5,000	EB07255	AB2291740	Everest Biotech	-
rabbit, polyclonal anti-TH	1:30,000	R-148-50	AB2492931	Biosensis	Lewis et al., 1993
guinea pig, polyclonal anti-GnRH	1:30,000	#1018	-	Made in house	Hrabovszky et al., 2011
sheep, polyclonal anti-POMC	1:50,000	#41	-	Gift of Dr. Csaba Fekete	Péterfi et al., 2018
goat, polyclonal anti-OXB	1:10,000	sc-8071	AB653612	Santa Cruz Biotech	Skrapits et al., 2015

Figure 1. Development of a versatile 'IHC/LCM-Seq' method for spatial transcriptomic analysis of immunohistochemically identified neuron populations. *A*, efficient RNA protection achieved by 0.05% aluminon (ATA) or 2% polyvinyl sulfonate (PVSA) in archived sections. Free-floating sections fixed with 4% paraformaldehyde (PFA) were stored in cryoprotectant solution at −20 °C for 3 years prior to RNA isolation and quality assessment with an Agilent Bioanalyzer. *B*, efficient preservation of the RNA integrity number (RIN) during immunohistochemical (IHC) procedures *via* including either 0.05% ATA or 2% PVSA in buffers and antibody solutions. Note the lack of effect of lower RNase inhibitor concentrations. *C*, impacts of 0.05% ATA and 2% PVSA on IHC signal and background levels using five different polyclonal antibodies against neurotransmitter marker enzymes (ChAT and TH) and neuropeptides (GnRH, OXB, POMC). While ATA tends to cause nonspecific labeling of cell nuclei and reduces IHC signals, adverse effects are avoided using PVSA. Scale bars represent 100 µm in low-power images and 25 µm in high-power insets. *$p < 0.0001$ by one-way ANOVA followed by Tukey's *post hoc* tests. ARC, Arcuate nucleus of the hypothalamus; Asterisk, third cerebral ventricle; Cc, corpus callosum; ChAT, choline-acetyltransferase; CPU, caudate-putamen; GnRH, gonadotropin-releasing hormone; LHA, lateral hypothalamic area; OXB, orexin B; POA, preoptic area; POMC, proopiomelanocortin; RRID, research resource identifier; TH, tyrosine hydroxylase.

transgenic mice (10). This method relied on the stabilization of the fluorescent ZsGreen marker protein *via* the transcardiac perfusion of mice with 0.5% PFA. RNA isolation from ∼300 to 330 cholinergic neurons visualized in 12-µm-thick coronal sections provided ∼1 ng total RNA. Ribosomal RNA depletion followed by random primer-based library preparation and Illumina sequencing of striatal cholinergic interneurons (ChINs) resulted in a reference transcriptome we used here for comparison with data to be obtained from the same cell type with IHC/LCM-Seq.

LCM-Seq studies of immunostained GnRH neurons

Use of IHC/LCM-Seq reproduces the main features of the reference ChIN transcriptome

Three mouse brains were fixed by transcardiac perfusion with 4% PFA and infiltrated with 20% sucrose. Twenty-µm-thick free-floating sections containing the dorsal striatum were prepared with a cryostat and ChINs were detected with IHC using antibodies against ChAT. The signal was visualized with the ABC technique and nickel-diaminobenzidine (Ni-DAB) chromogen (Fig. 2*A*). The IHC protocol used 2% PVSA in antibody solutions and buffers (except for the peroxidase developer), and primary antibodies were used at 4 °C as a precaution to maximize RNA preservation. Subsequent incubations were carried out at room temperature (Fig. 2*A*). After the peroxidase signal was developed, the sections were mounted on 'PEN' membrane-coated microscope slides from Elvanol containing 2% PVSA, air-dried, and then prepared and processed for LCM as detailed earlier (10). Approximately, 1000 immunostained ChINs were microdissected and pooled from the dorsal striatum of each brain (Fig. 2*A*). RNA preparation with the Arcturus Paradise Plus FFPE kit resulted in 3.3 ± 0.7 pg/neuron total RNA (mean ± SEM) with a RIN of 5.3 ± 0.2 (mean ± SEM) in three independent ChIN samples. These quantitative and qualitative measures were similar to the input parameters of the TruSeq Stranded Total RNA Library Preparation Gold kit in our previous LCM-Seq studies which used 300 to 330 laser-microdissected fluorescent ChINs (Total RNA: 3.8 ± 1.0 pg/neuron; RIN: 5.5 ± 0.4) (10). This kit is suitable for processing low-quality/low-quantity RNA samples and includes hybridization-based removal of rRNA sequences, followed by random primer-based reverse transcription of RNA transcripts (Fig. 2*A*) (10, 16–18). Twenty microliters of a 1 nM library mix representing proportionally the indexed cDNA samples was subjected to single-end sequencing with the Illumina NextSeq500/550 High Output kit (v2.5; 75 Cycles) and an Illumina NextSeq500 instrument (Fig. 2*A*), followed by bioinformatic analysis. The reference transcriptome was available for meta-analysis in BioProject with an accession number PRJNA901862 and new data were deposited with the accession number PRJNA1131978.

Sequencing of the three RNA-Seq libraries generated 37.3 M raw reads (11.3 M – 14.2 M per sample). After trimming with Trimmomatic and adapter removal with Cutadapt, mapping to the mouse reference genome (Ensembl; release 107) with STAR (v 2.7.11 b) resulted in 8.5 ± 0.5 M aligned reads from which 3.6 ± 0.3 M were assigned to unique genes and quantified with featureCounts (subread v 2.0.6). All transcripts, and the top 100 'receptors' (including G-protein-coupled receptors, cytokine receptors, nuclear receptors, and pattern recognition receptors) ranked by counts per million (CPM) values and 'ion channels', according to functional categories defined in the KEGG BRITE database, are reported in Table S1.

Library complexity and sensitive detection of low-abundance transcripts strongly depend on the amounts of input RNA and become compromised using 30 instead of 300 microdissected fluorescent ChINs as a source to prepare RNA-Seq libraries (10). Using either 1000 immunostained neurons ($ChINs_{IHC}$) or 300 laser-microdissected fluorescent neurons ($ChINs_{ZsG}$) (10) as a source of input RNA, we found that the percentages of reads aligned to exonic, intronic, and intergenic sequences were highly similar (Fig. S1*A*) and reflected the typical patterns characteristic to this library preparation method (10, 19). The relationship between the ratios of reads assigned to exonic sequences by featureCounts and the percentages of detected genes in the two experiments is depicted in library complexity plots (Fig. S1*B*). The two types of ChIN transcriptome contained similar numbers of transcripts (N ≈ 16,000; Cut-off: Reads ≥ 5), confirming nearly identical sensitivity and transcriptome coverage provided by the reference LCM-Seq and the new IHC/LCM-Seq approaches (Figs. 2*B*, S1*C*, and Table S1). A ∼3.6-times deeper sequencing applied in the LCM-Seq study (10) resulted in higher transcript numbers that met the criteria of Reads ≥ 10 or Reads ≥20 (Fig. S1*C*). Detection precision and accuracy of RNA-Seq studies are important requirements in quantitative RNA-Seq studies (20, 21). IHC/LCM-Seq and the previous LCM-Seq (10) studies revealed comparable abundances of nine cholinergic marker transcripts (shown in CPM) in the $ChINs_{IHC}$ and $ChINs_{ZsG}$ transcriptomes, respectively (Fig. 2*B*). High detection precision of the new method gained further support from the 94 to 95% overlap between the most abundant 100 receptors (Fig. 2*C* and Table S1) and 100 ion channels (Fig. 2*D* and Table S1). The remaining 5 transcripts ranked higher than 100 in one of the databases also exhibited comparable expression levels in the $ChINs_{ZsG}$ and $ChINs_{IHC}$ transcriptomes (Fig. 2, *C* and *D* and Table S1), indicating minimal amplification bias during library preparation. Transcripts per million (TPM) values with reads normalized to both transcript length and sequencing depth within each sample are provided in Table S1.

IHC/LCM-Seq studies provide insight into the gene expression profile of rat and mouse GnRH neurons

After validating the IHC/LCM-Seq technique, we began to characterize the gene expression profile of immunostained GnRH neurons. GnRH neurons of male Wistar rats (N = 6) and male C57/Bl6 mice (N = 6) were labeled with IHC in floated sections of the preoptic area using 2% PVSA for RNA preservation. Three TruSeq libraries were prepared from both species, each derived from 500 GnRH neurons that were microdissected and pooled proportionally from two animals (Fig. 3*A*). Illumina sequencing followed by bioinformatic analysis resulted in 6.5 ± 0.5 M aligned reads in rats and 4.7 ± 1.6 in mice, from which 2.2 ± 0.1 M and 1.9 ± 0.6 M, respectively, were assigned to unique genes. Transcript abundances quantified with featureCounts (subread v 2.0.6) were reported in CPM units. It was not possible to use reliable normalization to transcript length because of inaccuracies in the rat Ensembl database (mRatBN7.2).

The number of identified GnRH neuron transcripts was 13,153 ± 91 (mean ± SEM) in rats and 14,249 ± 1337 in mice. *GnRH1* mRNA expression was twice as high in rats (mean CPM_{RAT}: 7891) as in mice (mean CPM_{MOUSE}: 3549; Fig. 3, *A*

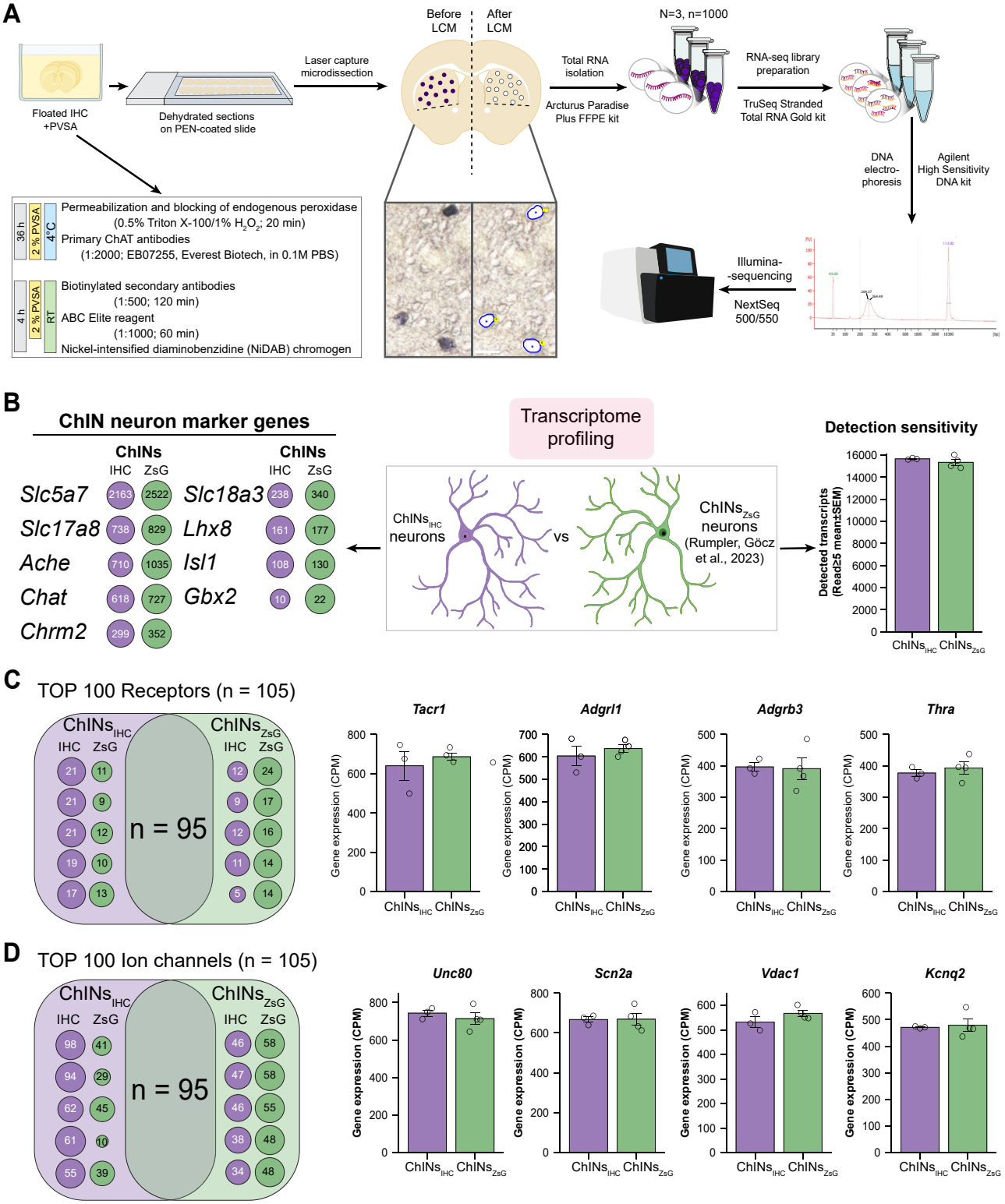

Figure 2. High similarity of the striatal cholinergic interneuron transcriptome characterized with IHC/LCM-Seq ($ChINs_{IHC}$) to the reference $ChINs_{ZsG}$ transcriptome obtained *via* LCM-Seq studies of ZsGreen-tagged ChINs of transgenic mice. *A*, schematics of the 'IHC/LCM-Seq' protocol to characterize the transcriptome profile of immunohistochemically labeled ChINs. *B*, comparative analysis of this transcriptome ($ChINs_{IHC}$) to a reference database ($ChINs_{ZsG}$) obtained with LCM-Seq from ChAT-Cre/ZsGreen transgenic mice. The same number of transcripts (Cut-off: Reads ≥ 5) detected in these independent studies indicates comparable sensitivity of the two approaches. Moreover, the IHC/LCM-Seq protocol and the reference LCM-Seq technique reveal similar relative abundances (shown in CPM units) of nine cholinergic marker transcripts, corroborating the precision and wide dynamic range of IHC/LCM-Seq. *C* and *D*, in further support of detection accuracy, Venn diagrams illustrate that 95% of the most abundant 100 receptors and ion channels are shared between the $ChINs_{IHC}$ and $ChINs_{ZsG}$ transcriptomes. The remaining five transcripts shown in dot plots also exhibit expression levels in the same order of magnitude (shown in CPM units). Column diagrams provide examples for highly expressed receptors and ion channels. For source data, see Table S1.

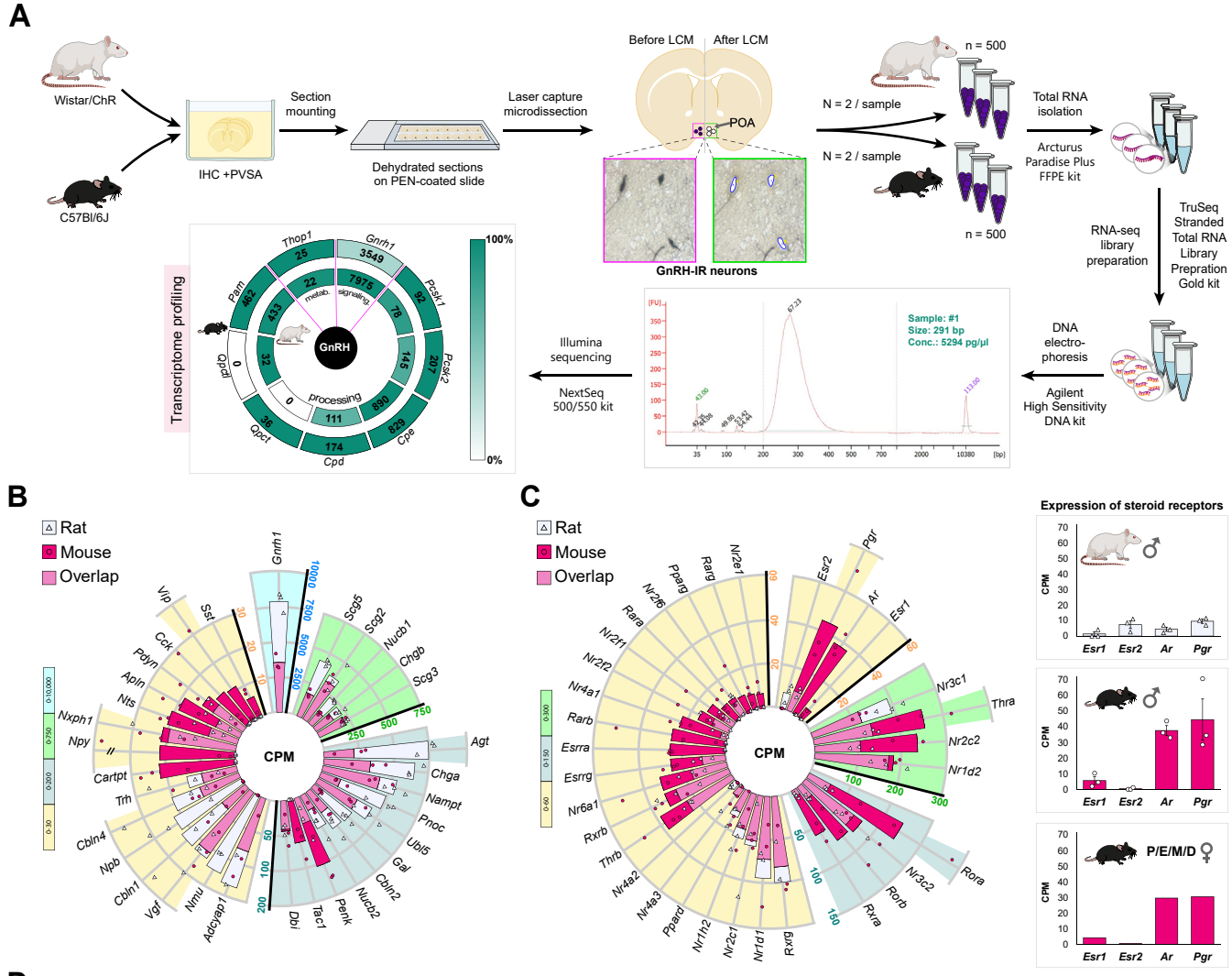

Figure 3. Characterization of the GnRH neuron transcriptomes from rats and mice using IHC/LCM-Seq. *A*, schematics of the optimized IHC/LCM-Seq protocol to characterize the GnRH neuron transcriptome from male rodents. Circle diagram illustrates in a comparative manner the expression levels (in CPM units) of *GnRH1* mRNA and enzyme transcripts catalyzing GnRH biosynthesis and degradation. *B*, transcripts encoding neuropeptides/granins are shown on radial column charts with different color-coded scales. In addition to neuropeptide cotransmitters shared between the two species, the *Nmu*, *Npb*, *Tac1*, and *Gal* transcripts dominate in rat and the *Npy*, *Cartpt*, and *Vip* transcripts dominate in mouse GnRH neurons. *C*, RNA-Seq experiments reveal intriguing species differences in the expression pattern of nuclear receptor transcripts. In particular, male rat GnRH neurons express exclusively *Esr2*, and male mouse GnRH neurons express exclusively *Esr1*. A mixed GnRH neuron sample pooled from different estrous cycle stages of female mice exhibits the same steroid receptor profile with selective expression of the *Esr1* estrogen receptor isoform. *D*, the expression level of G-protein–coupled receptors exhibit similarities as well as unique species-specific features in GnRH neurons of the two rodents. Underlining's delineate genes that differ by at least a factor of 2 in the two species (P, proestrus; E, estrus; M, metestrus; D, diestrus). For source data, see Table S2.

and *B*). The neurons contained the transcripts of known GnRH peptide processing (*Pcsk1*, *Pcsk2*, *Cpe*, *Cpd*, *Qpct*, *Qpctl*, *Pam*) and degrading (*Thop1*) enzymes, with the interesting species difference that the glutaminyl-peptide cyclotransferase activity could be attributed exclusively to *Qpctl* in rats and to *Qpct* in mice (Fig. 3*A*). While the analysis of neuropeptides and granins (defined in the peptide database: http://www.neuropeptides.nl/) detected similar levels of the *Scg2*, *Scg3*, *Nampt*, *Ubl5*, *Dbi*, *Nxph1*, and *Vgf* transcripts, other mRNAs showed different abundances in the two species. Only rat GnRH neurons cosynthesized neuromedine U (*Nmu*), neuropeptide B (*Npb*), and they expressed considerably higher levels of Substance P (*Tac1*) and galanin (*Gal*) than mice. In contrast, neuropeptide Y (*Npy*), cocaine- and amphetamine-regulated transcript (*Cartpt*), and vasoactive intestinal polypeptide (*Vip*) mRNAs were expressed dominantly in murine GnRH neurons (Fig. 3*B* and Table S2). As a general tendency, nuclear hormone receptors (Fig. 3*C* and Table S2) showed higher levels of expression in mice than in rats (*Thra, Nr2c2, Rora, Rorb, Rxra, Ar, Pgr*) (Fig. 3*C* and Table S2). Rat GnRH neurons expressed the beta estrogen receptor isoform (ERβ; *Esr2*) and were devoid of the classical alpha estrogen receptor (ERα; *Esr1*) (Fig. 3*C* and Table S2), in accordance with the previous *in situ* hybridization (4) and IHC (22) results from this species. Mouse GnRH neurons, in contrast, were entirely devoid of the *Esr2* transcript but expressed *Esr1* (Fig. 3*C* and Table S2). This finding was in conflict with the results of earlier scRT-PCR experiments which succeeded in amplifying *Esr2* (3) but not *Esr1* (23) from GnRH neurons of female mice, with estrous cycle-dependent changes in the percentages of *Esr2*-expressing GnRH neurons (6% in diestrus, 0% in proestrus, and 19% in estrus) (3). As our present study used male mice, we have addressed the possibility that the selective expression of *Esr1* in murine GnRH neurons stems from a sex difference. Therefore, we repeated the RNA-Seq experiments from a mixed cDNA sample generated from 500 GnRH neurons pooled proportionally from four female mice, each sacrificed at a different reproductive cycle stage (diestrus, proestrus, estrus, and metestrus; 10.00 AM). GnRH neurons of female mice in this control study also express ERα (*Esr1*) and were devoid of the *Esr2* transcript (Fig. 3*C* and Table S2).

G protein-coupled receptors (GPCRs) of GnRH neurons (Fig. 3*D* and Table S2) included adhesion GPCRs (*Adgrb1-3*, *Adgrl1-3*, *Adgrg1*, *Celsr1-3*…), adenosine receptors (*Adora1*, *Adora2a*…), adrenergic receptors (*Adra1a*, *Adra2c*…), muscarinic acetylcholine receptors (*Chrm1-4*), chemokine receptors (*Cx3cr1*), dopamine receptors (*Drd1-2*), type-1 cannabinoid receptor (*Cnr1*), type B endothelin receptor (*Ednrb*), metabotropic GABA (*Gabbr1-2*) and glutamate (*Grm1-5*; *Grm7-8*) receptors, serotonin receptors (*Htr1a*, *Htr1b*, *Htr2a*, *Htr2c*, *Htr4*, *Htr5a*…), histamine receptors (*Hrh1-3*), purinoceptors (*P2ry1, 4*; *P2ry12–13*…), taste (*Tas1r2*)- and vomeronasal receptors (*Vmn2r23–24*, *Vmn2r84–85*; *Vom1r46–47*, *Vom2r44*, *Vom2r66*...), receptors to various neuropeptides, including kisspeptins (*Kiss1r*), PACAP (*Adcyap1r1*), neurotensin (*Ntsr2*), calcitonin (*Calcr*), somatostatin (*Sstr1-2*), galanin (*Galr1*), thyrotropin-releasing hormone (*Trhr*), hypocretin-2 (*Hcrtr2*), Substance P (*Tacr1*), neurokinin B (*Tacr3*) and opioid peptides (*Oprd1, Oprl1, Oprm1*), and a large number of orphan receptors (*Gpr26, Gpr37, Gpr137, Gpr153, Gpr158, Gpr162*…; Fig. 3*D* and Table S2). Some receptor levels showed clear differences in the two species, including the dominance of the type-1 (*Chrm1*), type-3 (*Chrm3*), and type-4 (*Chrm4*) muscarinic acetylcholine receptors in mouse, and the type-2 receptor (*Chrm2*) in rat GnRH neurons (Fig. 3*D* and Table S2).

Neurotensin excites murine GnRH neurons via *acting on NTS2 receptors*

Kisspeptin is the most critical neuropeptide transmitter in the excitatory regulation of GnRH neurons. While studying GPCR transcripts, abundant expression of the specific kisspeptin receptor (*Kiss1r*) was confirmed (mean CPMs: 65.9 in rats and 58.8 in mice; Fig. 3*D*). Interestingly, GnRH neurons expressed similarly high levels of the type-2 neurotensin receptor (NTS2) transcript *Ntsr2* (mean CPMs: 45.1 in rats and 50.0 in mice; Fig. 3*D*). To address how this heavily expressed receptor contributes to the regulation of GnRH neuronal activity, we carried out whole-cell current-clamp studies (Fig. 4*A*) on male GnRH-GFP transgenic mice (24). We found that a single bolus of neurotensin (500 nM) increased the spontaneous firing rate of GnRH neurons to 197.6 ± 27.13% (mean ± SEM) of the control frequency (1.2 ± 0.21 Hz; (Fig. 4, *B* and *D and* Table S3)). To confirm the contribution of NTS2 to this effect, brain slices were preincubated with the subtype-specific NTS2 antagonist NTRC-824 (1 μM) prior to bolus application of neurotensin (Fig. 4*C*). NTRC-824 which had no significant effect on the firing rate when applied alone entirely prevented the excitatory effect of neurotensin (Fig. 4, *C* and *D* and Table S3). These functional observations provided evidence that the heavy *Ntsr2* expression plays an important role in the excitatory afferent control of GnRH neurons.

Adult GnRH neurons highly express genes implicated in fertility disorders

Rare genetic diseases affecting the normal development and/or functions of GnRH neurons cause pubertal disturbances and hypogonadotropic hypogonadism (HH) (25). While GnRH neurons likely express some of the HH disease genes only temporarily during development, other transcripts may persist into adulthood and contribute to the regulation of reproductive functions. In search of known HH transcripts in the adult GnRH neuron transcriptome, we studied the JAX (https://www.informatics.jax.org/disease), OMIM (https://www.omim.org/), and DO (https://disease-ontology.org/) public databases and the review literature (25) and identified 28 known disease genes that were expressed highly in adult GnRH neurons (Cut-off: mean CPM ≥ 5). These genes and associated clinical symptoms (OMIM references) are presented in Figure 5. It is reasonable to propose that the GnRH neuron transcriptome revealed in this IHC/LCM-Seq study contains additional fertility disease genes which need to be identified by clinical genetic research.

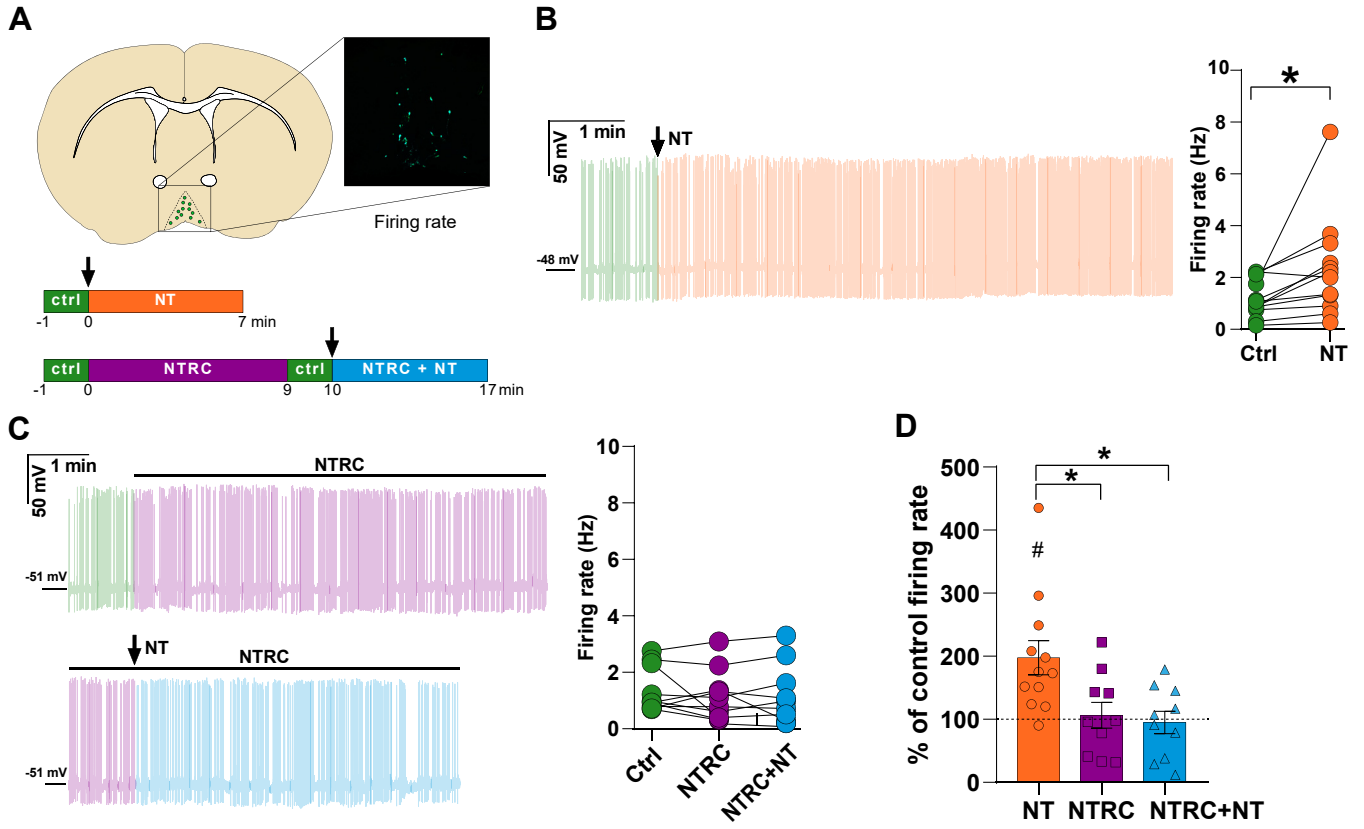

Figure 4. NTS2-mediated excitatory regulation of murine GnRH-GFP neurons by neurotensin. *A*, use of whole-cell patch-clamp electrophysiology in GnRH-GFP transgenic mice to study the NTS2-mediated effects of neurotensin (NT) on GnRH neuronal activity. *B*, representative recording of the excitatory response of a GnRH neuron to neurotensin (NT, 500 nM). Graph illustrates the firing rates of individual neurons before (Ctrl) and after (NT) bath application of NT, with a significant increase in neuronal activity (Hz). *C*, GnRH neuron firing before and after sequential bath application of the NTS2 antagonist NTRC-824 (NTRC; 1 μM) and NT. Representative traces and the chart with the firing rates of individual neurons reveal that NTRC-824 has no effect on the spike frequency of GnRH-GFP neurons, whereas it prevents entirely the excitatory effect of NT. *D*, bar graph summarizing the effects of NT, NTRC alone, and the sequential application of NTRC and NT on GnRH neuronal firing expressed as the percentages of control firing rates. *$p < 0.05$. For source data and statistics, see Table S3.

Discussion

The goal of this study was the development and validation of a versatile, sensitive, and accurate IHC/LCM-Seq method which can be readily used for gene expression profiling of any neuronal phenotype visualized with IHC in tissue sections of brains fixed with 4% PFA. Using this methodology, we have characterized the detailed transcriptome profile of rat and mouse GnRH neurons.

In a reference LCM-Seq method we reported recently, we collected and pooled fluorescently tagged cholinergic neurons from 0.5% PFA-fixed and slide-mounted 12-μm-thick sections (10). In that method, we used the Arcturus Paradise PLUS FFPE RNA Isolation Kit (Thermo Fisher Scientific) to isolate 1 to 2 ng total RNA with an RIN value of ∼5.5 from 300 to 330 neurons. The cDNA libraries were prepared with the TruSeq Stranded Total RNA Library Preparation Gold kit (Illumina). RNA-Seq using an Illumina NextSeq500 instrument and the NextSeq500/550 v2.5 kit enabled us to detect over 15,000 different transcripts (Cut-off: Reads ≥ 5) in spatially defined cholinergic cell populations (10). To reproduce these RNA input parameters in the new IHC/LCM-Seq protocol, major technical challenges we faced included i) the risk of increasing the concentration of PFA to 4%, ii) difficulties to preserve RNA integrity during long-term section storage, and in particular, iii) RNA protection during the IHC processing of free-floating tissue sections.

Standard IHC protocols on free-floating sections require the use of 4% PFA fixation for optimal tissue integrity and antigenicity. Against the general assumption that the quality and yield of RNA isolated from fixed tissues are not compatible with RNA-Seq experiments (26, 27), Bioanalyzer tests established that RNA extracted from 4% PFA-fixed 20-μm-thick sections can be surprisingly well-preserved (*e.g.*: RIN value of 8.3 ± 0.3 in the pre-IHC test). Further, we were able to extract 3.3 ng total RNA (3.3 pg/neuron) from 1000 immunostained and microdissected ChINs, allowing us to conclude that a few hundred immunostained neurons harvested from 4% PFA-fixed 20-μm-thick sections should provide sufficient amounts of RNA for subsequent cDNA library preparation and RNA-Seq experiments (10, 17, 18).

The major challenge of the IHC/LCM-Seq method was RNA preservation during long-term storage of tissue sections and IHC procedures. During method development, we considered and tested a variety of reagents, enzymes, and additives that were used in the past for RNA protection. For example, RNAlater solution (patented by Ambion) which can

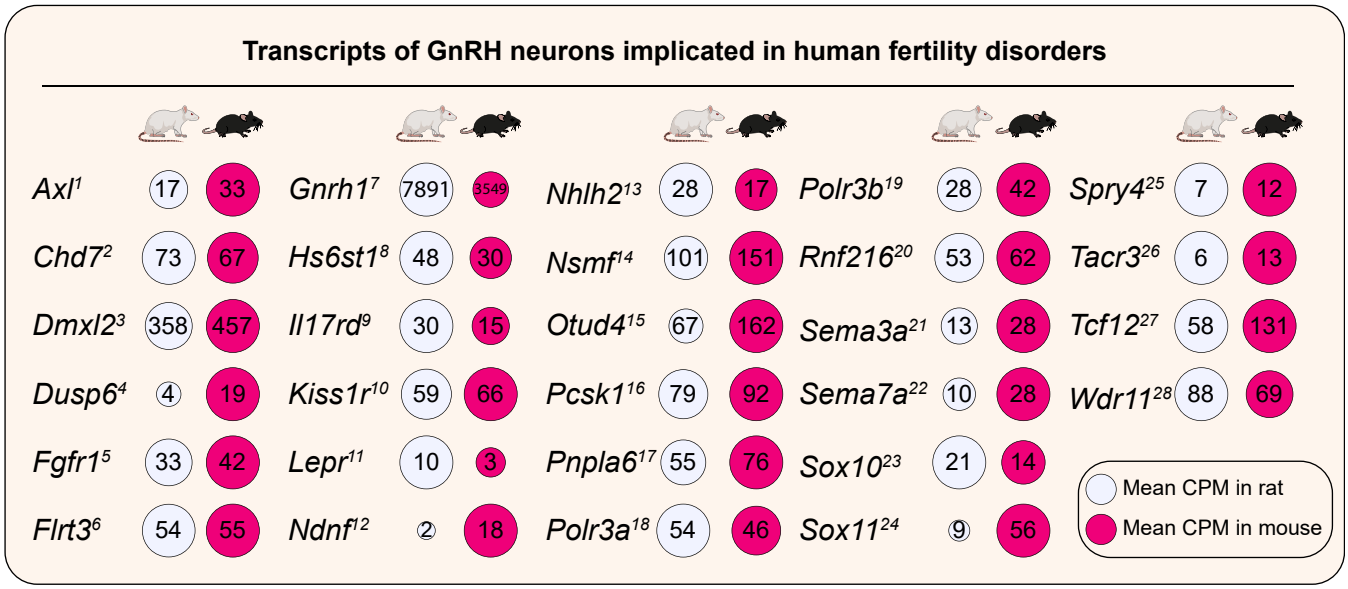

Figure 5. Genes implicated in congenital hypogonadotropic hypogonadism that are also expressed highly in GnRH neurons of adult rodents. 28 genes implicated in congenital hypogonadotropic hypogonadism based on the JAX (https://www.informatics.jax.org/disease), OMIM (https://www.omim.org/), and DO (https://disease-ontology.org/) databases and relevant review literature (25) are expressed highly in the GnRH neurons of adult rats and mice. For clinical symptoms, see OMIM references.

efficiently preserve RNA integrity during long-term tissue storage, histological blocks infiltrated with this reagent are difficult to section with a cryostat. Furthermore, the application of RNAlater is not compatible with IHC procedures (28, 29). Use of enzymatic RNase inhibitors (RNAsin, RNAgard, SUPERaseIN, RNaseOUT, etc) that were tried before to preserve RNA for various downstream applications, including qPCR (30, 31), microarray (32), and 10x Genomics (33), is impractical in antibody solutions and wash buffers due to their high costs (33). Ribonucleoside vanadyl complex (VRC) is a small molecule RNase inhibitor (34, 35) applied previously by others in RNA-Seq protocols (29, 36). VRC was reported to preserve an excellent RNA quality following even lengthy antibody incubations (29). Problems faced while using this approach were the presence of unspecific immunofluorescent signals, the poor contrast of the immunofluorescent images (33), and the interference of VRC remnants with downstream applications, including reverse transcription (29). Use of high-salt buffers in an attempt to protect RNA also tended to result in reduced immunofluorescent signals (29).

The general nuclease inhibitory activities of aluminon and PVSA have been known for many decades (13, 14). These inexpensive reagents can improve the quality and yield of RNA extraction even from RNase-rich tissues (37, 38). In pilot experiments to test these long-known reagents in our new application, we found that 0.05% aluminon and 2% PVSA can efficiently prevent the degradation of tissue RNAs during cryoprotectant storage and IHC incubations of PFA-fixed free-floating histological sections. We note that RNA protection by these reagents may become less efficient at higher temperatures and each specific IHC/LCM-Seq project may require further method optimization with the preferential use of 4 °C solutions. We found that the presence of aluminon in some antibodies compromised the IHC results, whereas addition of PVSA to the cryoprotectant solution caused clumping of stored tissue sections, indicating that optimal protocols should consist of a combined use of the two additives.

Previous Immuno-LCM methodologies followed by RNA-Seq relied on the use of alcohol-based precipitating (molecular) fixatives, coupled with various RNA-preserving strategies (29, 39, 40). The most common approach to minimize RNA degradation was rapid immunolabeling with incubation times shortened to a few minutes (39). This pulse labeling principle was combined successfully with the use of RNase inhibitors (SUPERase) and low temperatures (40). These published protocols have very limited sensitivity and use. Notably, alcohol extracts, instead of preserving short neuropeptides like GnRH (41) and therefore, cannot be used as a fixative for IHC/LCM-Seq studies of peptidergic neuronal systems. The high potential of our IHC/LCM-Seq method stems from the replacement of precipitating fixatives with the most versatile cross-linking fixative, buffered 4% PFA. Using transcriptomic studies of ChINs as a method test system, we could establish formally that the amount and the quality of RNA extracted from immunostained sections satisfy the input requirements of the TruSeq Stranded Total RNA Library Preparation Gold kit,

as determined in a previous LCM-Seq study on genetically labeled cholinergic neurons (10). This library preparation protocol we used successfully in both studies has been developed specifically for low-quality/low-quantity RNA samples and relies on the RiboZero technology to remove rRNA, followed by reverse transcription with random primers and then, enrichment of the cDNA fragments with PCR.

Fluorescence activated cell sorting of dispersed live neurons (42) provides an elegant alternative to LCM to harvest neurons for RNA-Seq studies. Comparison of these approaches in Table 1 delineates some unique advantages of IHC/LCM-Seq, which provides high spatial precision, alleviates the need for using transgenic mice, stabilizes the transcriptome profile which is critical for quantitative RNA-Seq experiments, and offers an intriguing possibility to study human neurons from formaldehyde-fixed autopsy material.

The transcriptome profile of genetically modified mouse GnRH neurons has already been studied successfully with microarray analysis of cytoplasmic samples collected with patch electrodes (5), LCM of fluorescently tagged GnRH neurons coupled with microarray analysis (6), and ribosome affinity purification coupled with RNA-Seq (7). IHC/LCM-Seq is the first high-throughput technique which also enabled deep transcriptome profiling of rat GnRH neurons with an unprecedented depth (13,000–14,000 transcripts at the Cut-off of Reads ≥ 5). While detailed discussion of findings is not possible in the frame of this technical paper, receptor profiles indicated that kisspeptin, PACAP, neurotensin, neuropeptide Y, substance P, neurokinin B, and opioid peptides contribute to the afferent control of GnRH neuronal functions, in addition to the classic neurotransmitters GABA, glutamate, acetylcholine, and monoamines. The functional significance of an unexpectedly high level of *Ntsr2* expression was assessed in slice electrophysiology experiments in which we established that neurotensin is a strong stimulator of GnRH neuronal activity. Neurotensin acting physiologically on NTS2 could partly originate from preoptic kisspeptin neurons (18) which innervate GnRH neurons. Presence of neurotensin immunoreactivity (43) and the *Nts* transcript (Fig. 3*B*) in GnRH neurons also raise the possibility that neurotensin from intrinsic sources regulates GnRH neurons *via* autocrine/paracrine mechanisms.

We propose that several orphan receptors we identified in GnRH neurons may become future drug targets to influence reproduction. Due to the high sensitivity of bulk sequencing from 500 pooled GnRH neurons, we were able to study sex steroid receptors which only occur at low abundances in GnRH neurons. In an influential study in 1983, Shivers et al. reported that the cell nuclei of rat GnRH neurons are unable to take up tritiated estradiol (44), giving rise to the concept that gonadal sex steroids mostly exert feedback effects on GnRH neurons indirectly *via* interneurons containing estrogen receptors (ERα and ERβ). Given that most ERβ-KO mouse models are fertile, whereas ERα-KO mice are not (45), the classical ERα receptor form appears to play dominant role in the regulation of the GnRH neuronal system both during negative feedback and the temporary positive E2 feedback (46) which triggers the mid-cycle surge of GnRH/luteinizing hormone. The possibility of some direct estrogen signaling to GnRH neurons was revisited in 1999 by single cell multiplex RT-PCR studies which amplified the estrogen receptor transcripts from the cytoplasm of individual GnRH neurons of mice (3). Our *in situ* hybridization studies in 2000 (4) with an improved methodology (47) have established that GnRH neurons of the rat express only the ERβ receptor form (at the given detection sensitivity), which was confirmed later with IHC (22). A single-cell RT-PCR study repeated later concluded that ERβ is the only estrogen receptor form expressed by GnRH neurons also in mice (23). Generalized statements about rodent species (23) formed today's view that in both rodents, the direct effects of E2 on GnRH neurons exclusively involve the ERβ receptor form (48). In contrast with this opinion, our IHC/LCM-Seq studies were only able to detect the ERα transcript (*Esr1*) in the GnRH neurons of both male and female mice. We note that an earlier RNA-Seq study of affinity-purified translating ribosomes isolated from murine GnRH neurons also found higher levels of the *Esr1 versus* the *Esr2* transcripts in the GnRH-enhanced RNA pool (7).

We propose that the gene expression profile of GnRH neurons opens the way for new strategies to influence the reproductive axis. High levels of expression of known infertility genes in GnRH neurons may explain the pathomechanisms of some clinical cases of HH. Further, the transcriptome profiles may also promote the discovery of new disease genes causing human cases of HH.

A technical problem we faced while we characterized the rat GnRH neuron transcriptome stemmed from multiple inaccuracies in the GTF files downloaded from Ensembl. Using the latest rat genome release (mRatBN7.2), the Ensembl genome browser identified 14 exons in the rat *Gnrh1* gene with a

Table 1
Comparison of fluorescence-activated cell sorting (FACS) and laser capture microdissection (LCM) to collect cells for RNA-Seq experiments

Feature	FACS	IHC/LCM-Seq
Throughput	High	High
Cell viability	Live sorted cells	Fixed cells
Spatial information	Lost	Preserved
RNA quality	May be affected	Slightly compromised
Source of possible sample contamination	Cell clumping	Microenvironment of dissected cells
Library preparation	Oligo(dT)-based	Random primer-based (*e.g.* RiboZero)
Transcriptome stability	May change during cell sorting	Preserved as a physiological snapshot
Use on animal tissues	Requires fluorescent markers	No need for fluorescent tags
Use on *post mortem* brain	Not compatible	Potentially adaptable

summed transcript length of 7784 bases. In contrast, the NCBI database indicated more realistically that the rat *Gnrh1* gene contains four exons, giving rise to a total transcript length of 505 bases, very close to the length of the mouse *Gnrh1* transcript (642 bases in the Ensembl and 483 bases in the NCBI databases). Similar problems in determining the transcript length of other rat genes from the GTF files used by featureCounts warned us against using TPM normalization while comparing the GnRH neuron transcriptome between the two rodent species and we report CPM values which compensate only for differences in sequencing depth.

In conclusion, we developed, validated, and used a versatile 'IHC/LCM-Seq' method and carried out spatial transcriptome profiling of GnRH neurons visualized with IHC in the hypothalamic sections of rats and mice. Use of regular 4% PFA fixation in this protocol allows the detection of various neuronal phenotype markers. IHC/LCM-Seq can be used in any species, unlike previously developed high-throughput approaches which require genetic modifications available mostly in mice. Owing to the bulk sequencing approach, nanogram amounts of input RNA renders IHC/LCM-Seq similarly sensitive (∼15,000 transcripts detected per cell type) and accurate as the reference LCM-Seq protocol we reported earlier to characterize genetically tagged cholinergic neurons of transgenic mice (10). Importantly, the potent RNase inhibitors aluminon and PVSA we introduced for this new application can efficiently prevent RNA degradation during long-term storage and IHC processing of histological sections. Compatibility of the new IHC/LCM-Seq method with formaldehyde fixation also opens new perspectives for human research. Provided RNA degradation can be limited during the *post mortem* period, the IHC/LCM-Seq method offers a possibility to characterize the transcriptome profile of various human cell types with spatial precision using either healthy or pathological autopsy samples. Future adaptation of the method to FFPE tissues used in routine histopathology may extend further the application of IHC/LCM-Seq method to other organs and tissues.

Experimental procedures

Animals

Animal experiments were carried out in accordance with the Institutional Ethical Codex, Hungarian Act of Animal Care and Experimentation (1998, XXVIII, section 243/1998) and the European Union guidelines (directive 2010/63/EU) and approved by the Animal Care and Use Committee of the HUN-REN Institute of Experimental Medicine. All efforts were made to minimize potential pain or suffering and to reduce the number of animals used. Adult C57/BL6 male (∼3 month old; N = 23) and female (3–5 months old; N = 4) mice, Wistar Charles River rats (∼3 months old; N = 6), and GnRH-GFP transgenic mice (∼3 months old; N = 8) (24) were housed under standard conditions (lights on between 0700 and 1900 h, temperature 22 ± 1 °C, chow and water *ad libitum*) in the animal facility of the HUN-REN Institute of Experimental Medicine.

Perfusion fixation

Rats (N = 6) and mice (N = 27) were anesthetized with a cocktail of ketamine (25 mg/kg), xylavet (5 mg/kg), and pipolphen (2.5 mg/kg) in saline and perfused transcardially with 50 ml of freshly prepared ice-cold 4% PFA in 0.1 M PBS (PBS; 0.1 M; pH 7.4). Following a 5-h-postfixation in this fixative, the brains were infiltrated overnight with sterile 20% sucrose solution in PBS, snap-frozen on powdered dry ice, and stored at −80 °C until sectioned with a cryostat.

Section preparation

For all experiments, reagents were of molecular biology grade. The MQ water and PBS were pretreated overnight with diethylpyrocarbonate (Thermo Fisher Scientific; 1 ml/L) and autoclaved. Other solutions were prepared using diethylpyrocarbonate-treated and autoclaved MQ water. The working area was cleaned with RNaseZAP (Merck KGaA). Brains were sectioned at 20 μm in the coronal plane with a Leica CM1860 UV cryostat (Leica Biosystems). Sections corresponding to plates 28 to 36 of the Rat Brain Atlas of Paxinos and Watson (Bregma +0.60 to −0.36 mm) (49) and to plates 20 to 46 of the Mouse Brain Atlas of Paxinos and Franklin (Bregma +1.33 to −1.79 mm) (50) were stored at −20 °C in cryoprotectant (antifreeze) solution (30% ethylene glycol; 25% glycerol; 0.05 M phosphate buffer; pH 7.4) with or without the additives 0.05% aluminon (13) or 2% PVSA (14).

RNA extraction and analytics

RNA samples (N ≥ 3/group) were prepared with the PureLink FFPE Kit (Thermo Fisher Scientific) from whole brain sections and with the Arcturus Paradise PLUS FFPE RNA Isolation Kit (Applied Biosystems) from microdissected cholinergic and GnRH neurons. RNA yield and integrity number (RIN) were studied with the Agilent 2100 Bioanalyzer system using the Eukaryotic Total RNA Pico Chips and the 2100 Expert software (Agilent).

Testing of RNA quality after long-term storage of tissue sections

Free-floating sections from the brains of three male mice were stored for 3 years at −20 °C in aqueous cryoprotectant solutions supplemented with RNase inhibitors (0.05% aluminon or 2% PVSA), whereas control sections were kept in cryoprotectant without additives. Then, three whole sections from each group (1 section/mouse) were used for total RNA isolation (PureLink FFPE Kit) and Bioanalyzer testing. After confirming normality with the Shapiro–Wilk test, the RIN values of the three treatment groups were compared by one-way ANOVA followed by Tukey's *post hoc* test.

Effects of RNase inhibitors on RNA integrity during IHC

All reagents and buffers were maintained under RNase-free, sterile conditions with or without the additional use of the RNase inhibitors aluminon (0.0005%, 0.005%, or 0.05%; m/V)

or PVSA (1 or 2%; V/V) in buffers and antibody solutions. Floated sections corresponding to plates 24 to 32 of the Mouse Brain Atlas of Paxinos and Franklin (Bregma +0.85 to −0.11 mm) (50) from 3 to 8 brains were thoroughly rinsed in PBS, pretreated with 1% H_2O_2 and 0.5% Triton X-100 for 20 min, and then processed for the peroxidase-based IHC detection of GnRH neurons using previously characterized polyclonal GnRH antibodies raised in a guinea pig (#1018; 1: 30,000; 35h; 4 °C) (15). Primary antibodies were reacted with Biotin-SP-AffiniPure anti-guinea pig IgG (Jackson ImmunoResearch; 1:500; 2h; RT) and the ABC Elite reagent (Vector; 1:1000; 1 h; RT). The peroxidase enzyme reaction was visualized with Ni-DAB chromogen [10 mg diaminobenzidine, 30 mg nickel-ammonium-sulfate, 0.003% H_2O_2 in 20 ml Tris-HCL buffer solution (0.05 M; pH 8.0); RT]. All solutions, except for the developer, contained the RNase inhibitors 0.05% aluminon or 2% PVSA. 3 sections/treatment were used for RNA isolation with the PureLink FFPE Kit. Quality assessments were carried out before and after IHC using the RNA 6000 Pico Kit with the Agilent 2100 Bioanalyzer System. Normality of RIN data was evaluated using the Shapiro–Wilk test. The RIN values of the post-IHC groups were compared by one-way ANOVA followed by Tukey's *post hoc* tests.

Effect of 0.05% aluminon and 2% PVSA on the quality of IHC signals

Twenty-µm-thick sections corresponding to plates 20 to 46 of the Mouse Brain Atlas of Paxinos and Franklin (Bregma +1.33 to −1.79 mm) (50) were collected with a cryostat from the 4% PFA-fixed brains of three mice. Rinse buffers and IHC reagents (except for the peroxidase developer) were supplemented with the RNase inhibitors 0.05% aluminon or 2% PVSA. The sections were thoroughly rinsed in PBS and pretreated with 1% H_2O_2 and 0.5% Triton X-100 for 20 min. For IHC experiments, they were incubated for 35 h at 4 °C in one of the following primary antibodies: goat anti-ChAT (EB07288; RRID: AB2291740; Everest Biotech; 1:5000), rabbit anti-TH (R-148-50; RRID: AB2492931; Biosensis; 1:30,000), guinea pig anti-GnRH (#1018; 1:30,000) (15), goat anti-POMC (#41; Gift of Dr Csaba Fekete; 1:50,000) (51), and goat anti-OXB (sc-8071; RRID: AB653612; Santa Cruz Biotech; 1:10,000) (52). Following PBS rinses, biotinylated secondary antibodies raised in donkeys (Jackson ImmunoResearch; 1:500; 2h; RT) and the ABC Elite reagent (Vector; 1:1000; 1 h) were applied to the sections at RT and the peroxidase signals were visualized with Ni-DAB chromogen [10 mg diaminobenzidine, 30 mg nickel-ammonium-sulfate, 0.003% H_2O_2 in 20 ml Tris–HCL buffer solution (0.05 M; pH 8.0)]. Immunostained sections were mounted on microscope slides, air-dried, dehydrated with 70%, 95%, and 100% ethanol (5 min each), cleared with xylenes (2 × 5 min), and coverslipped with DPX mounting medium (Merck) for light microscopic analysis and photography. Digital images were corrected for brightness/contrast using Adobe Photoshop (Adobe Systems) and the final composite figures were prepared with Adobe Illustrator (Adobe Systems).

Transcriptomic studies of immunostained ChINs

Perfusion fixation and section preparation

Brains of three adult male mice were perfusion-fixed with 4% PFA, postfixed, infiltrated with 20% sucrose, and snap-frozen on pulverized dry ice as described above. Twenty-µm-thick sections containing the CPU (Atlas plates 20–26 of Paxinos and Franklin; Bregma +1.33 to +0.61 mm) (50) were placed in 0.05% aluminon-containing antifreeze solution (30% ethylene glycol; 25% glycerol; 0.05 M phosphate buffer; pH 7.4) and stored at −20 °C until processed for ChAT IHC.

IHC detection of ChINs in the dorsal striatum

All reagents and buffers were kept under sterile conditions to minimize RNase exposure and, except for the peroxidase developer, contained 2% PVSA to inhibit RNases. Floated sections were thoroughly rinsed in PBS, pretreated with 1% H_2O_2 and 0.5% Triton X-100 for 20 min, and then processed for the peroxidase-based IHC detection of ChINs in the dorsal striatum. For IHC, goat anti-ChAT antibodies (EB07255; RRID: AB2291740; 1:5000; 35 h; 4 °C), biotinylated secondary antibodies (Biotin-SP-AffiniPure anti-goat IgG; Jackson ImmunoResearch; 1:500; 2 h; RT), and the ABC Elite reagent (Vector; 1:1000; 1 h; RT) were used, and the peroxidase signal was developed with Ni-DAB chromogen [10 mg diaminobenzidine, 30 mg nickel-ammonium-sulfate, 0.003% H_2O_2 in 20 ml Tris–HCL buffer solution (0.05 M; pH 8.0); RT]. Immunostained sections were mounted onto PEN membrane glass slides (Membrane Slide 1.0 PEN, Carl Zeiss) from Elvanol, air-dried, and preprocessed for LCM using sequential incubations in 70% (60 s), 96% (60 s), and 100% (2 × 60 s) ethanol, followed by xylenes (60 s). The slides were stored at −80 °C in slide mailers with silica gel desiccants, unless processed immediately for LCM.

LCM of immunostained ChINs

ChAT-positive neurons were microdissected individually and pressure-catapulted into 0.5 ml tube caps (Adhesive Cap 200, Carl Zeiss) with a single laser pulse using a 40 × objective lens and the PALM Microbeam system and RoboSoftware (Carl Zeiss). 1000 neurons/group pooled from the dorsal striatum were stored in the LCM tube caps at −80 °C until RNA extraction.

RNA extraction and analytics

RNA samples were prepared with the Arcturus Paradise PLUS FFPE RNA Isolation Kit (Applied Biosystems). Each sample (N = 3) included 1000 ChINs. RNA yield/neuron and RIN values were provided as mean ± SEM of the three samples.

RNA-Seq library preparation

Sequencing libraries were prepared with the TruSeq Stranded Total RNA Library Preparation Gold kit (Illumina) from 1000 immunostained cholinergic neurons microdissected and pooled from the dorsal striatum. The 15 PCR cycles

recommended by the manufacturer for DNA fragment enrichment were increased to 16 using 1000 neurons (16, 17). A 1 nM library mix (120 µl) containing proportionally three indexed samples was sequenced with an Illumina NextSeq500 instrument using the NextSeq500/550 High Output v2.5 kit (75 cycles) to obtain the $ChINs_{IHC}$ transcriptome which was compared to the $ChINs_{ZsG}$ reference transcriptome (10).

Bioinformatics

Trimmomatic 0.39 (settings: LEADING:3, TRAILING:3, SLIDINGWINDOW:4:15, MINLEN:36) (53) and Cutadapt 4.6 (54) were used to remove low quality and adapter sequences, respectively. Remaining reads were mapped to the Ensembl mm107 mouse reference genome using STAR (v 2.7.11 b) (55). Read assignment to genes, read summarization, and gene level quantification were performed by featureCounts (Subread v 2.0.6) (56). The CPM values were calculated with the edgeR R-package (57). Transcript lengths data to calculate TPM values were obtained from the Ensembl GTF file. Transcriptome coverage was defined as the number of different transcripts (Cut-off: reads ≥ 5) in each sample and presented as the mean ± SEM of three transcriptomes.

Functional classification of $ChINs_{IHC}$ and $ChINs_{ZsG}$ transcripts

Transcripts present at a mean CPM≥1 in either the $ChINs_{IHC}$ or the $ChINs_{ZsG}$ (10) transcriptomes were arranged by mean CPMs and listed in Table S1, together with the top 100 transcripts in the *Ion channels* and *Receptors* KEGG BRITE categories. Some manually selected markers of cholinergic neurotransmission were illustrated in dot plots.

IHC/LCM-Seq studies of GnRH neurons

Section preparation

Twenty-µm-thick sections containing the preoptic area of the hypothalamus [(plates 28–36 of the Rat Brain Atlas of Paxinos and Watson; Bregma +0.60 to −0.36 mm) (49) and plates 24–32 of the Mouse Brain atlas of Paxinos and Franklin; Bregma +0.85 to −0.11 mm)] (50) were stored at −20 °C in 0.05% aluminon-containing antifreeze solution (30% ethylene glycol; 25% glycerol; 0.05 M phosphate buffer; pH 7.4) until processed for the IHC detection of GnRH.

IHC detection of GnRH neurons

Reagents and buffers (except for the peroxidase developer) contained 2% PVSA to inhibit RNases. Floated sections were thoroughly rinsed in PBS and pretreated with 1% H_2O_2 and 0.5% Triton X-100 for 20 min. They were immunostained using sequentially guinea pig anti-GnRH antibodies (#1018; 1:30,000; 35h; 4 °C) (15), biotinylated secondary antibodies (Biotin-SP-AffiniPure anti-guinea pig IgG; Jackson ImmunoResearch; 1:500; 2h; RT), and the ABC Elite reagent (Vector; 1:1000; 1 h; RT), followed by the chromogen solution which was devoid of PVSA [10 mg diaminobenzidine, 30 mg nickel-ammonium-sulfate, 0.003% H_2O_2 in 20 ml Tris–HCL buffer solution (0.05 M; pH 8.0); RT]. The immunostained sections were mounted onto PEN membrane glass slides (Membrane Slide 1.0 PEN, Carl Zeiss), air-dried, and preprocessed for LCM using sequential incubations in 70% (60 s), 96% (60 s), and 100% (2 × 60 s) ethanol, followed by xylenes (60 s). The sections were either stored at −80 °C in slide mailers with silica gel desiccants or processed immediately for LCM.

LCM of immunostained GnRH neurons

Immunolabeled GnRH neurons of rats (N = 6, N = 2/groups) and mice (N = 6; N = 2/groups) were microdissected individually and pressure-catapulted into 0.5 ml tube caps (Adhesive Cap 500, Carl Zeiss) as described above. Five hundred neurons pooled from the hypothalamic preoptic area of two animals were stored in the LCM tube caps at −80 °C until RNA isolation.

An additional control experiment used a mixed library prepared proportionally from 500 neurons of four female mice, representing each of the estrous, metestrous, diestrous, and proestrous cycle stages.

RNA extraction

RNA samples were prepared with the Arcturus Paradise PLUS FFPE RNA Isolation Kit (Applied Biosystems). To obtain sufficient amounts of RNA, each sample included 500 GnRH neurons pooled from two rat or mouse brains.

RNA-Seq library preparation

Sequencing libraries were prepared with the TruSeq Stranded Total RNA Library Preparation Gold kit (Illumina) from 500 immunostained GnRH neurons/group microdissected and pooled from the preoptic area of the rat and mouse hypothalami. The number of PCR cycles recommended by the manufacturer for DNA fragment enrichment was increased to 16 (17). A 1 nM library mix (120 µl) containing proportionally three indexed samples was sequenced with an Illumina NextSeq500 instrument using the NextSeq500/550 High Output v2.5 kit (75 cycles).

Bioinformatics

Trimmomatic 0.39 (settings: LEADING:3, TRAILING:3, SLIDINGWINDOW:4:15, MINLEN:36) (53) and Cutadapt 4.6 (54) were used to remove low quality and adapter sequences, respectively. Remaining reads were mapped to the Ensembl mm111 mouse reference genome using STAR (v 2.7.11b) (55). Read assignment to genes, read summarization, and gene level quantification were performed by featureCounts (Subread v 2.0.6) (56). The CPM values were calculated with the edgeR Bioconductor package (57). Transcriptome coverage was defined as the number of different transcripts (Cut-off: Reads ≥ 5) in each sample.

Functional classification of GnRH neuron transcripts

Transcripts present at CPM≥1 in the rat and mouse GnRH neuron transcriptomes were arranged by mean CPMs and also ranked by their presence in 3, 2, or only 1 of the three samples.

LCM-Seq studies of immunostained GnRH neurons

These results reflecting the transcriptional landscapes of rat and mouse GnRH neurons were listed in Table S2, with three selected functional categories (*neuropeptides, nuclear receptors, G-protein coupled receptors*) defined using the KEGG BRITE database. Some known GnRH peptide processing and degrading enzymes were selected manually and illustrated in circle diagram.

Slice electrophysiology

Brain slice preparation

Brain slices were prepared as described earlier (58) with slight modifications. GnRH-GFP transgenic mice (~3 months old; N = 7) (24) were decapitated in deep isoflurane anesthesia. The brain was immersed in ice-cold low-Na cutting solution bubbled with carbogen (mixture of 95% O_2 and 5% CO_2). This solution contained the following (in mM): saccharose 205, KCl 2.5, $NaHCO_3$ 26, $MgCl_2$ 5, NaH_2PO_4 1.25, $CaCl_2$ 1, glucose 10. Brain blocks including the preoptic area where GnRH neurons reside were dissected. 220-µm-thick coronal slices were prepared with a VT-1000S vibratome (Leica Biosystems) and transferred into oxygenated artificial cerebrospinal fluid (aCSF; 33 °C) containing (in mM) the following: NaCl 130, KCl 3.5, $NaHCO_3$ 26, $MgSO_4$ 1.2, NaH_2PO_4 1.25, $CaCl_2$ 2.5, glucose 10. The solution was then allowed to equilibrate to room temperature for 1 h.

Whole-cell patch clamp experiments

Recordings were carried out in oxygenated aCSF at 33 °C using Axopatch-200B patch-clamp amplifier, Digidata-1550B data acquisition system, and pClamp 10.7 software (Molecular Devices Co). Neurons were visualized with a BX51WI IR-DIC microscope (Olympus Co). GnRH-GFP neurons showing green fluorescence in the majority of GnRH neurons in the preoptic area of transgenic mice (24) were identified by a brief illumination (CoolLED, pE-100) at 470 nm using an epifluorescent filter set. The patch electrodes (OD = 1.5 mm, thin wall; WPI) were pulled with a Flaming-Brown P-97 puller (Sutter Instrument Co). Electrode resistance was 2 to 3 MΩ. The intracellular pipette solution contained (in mM) the following: KCl 140, Hepes 10, $CaCl_2$ 0.1, EGTA 5, Mg-ATP 4, Na-GTP 0.4. pH = 7.2 to 7.3 with NaOH. Pipette offset potential, series resistance (R_s), and capacitance were compensated before recording. Only cells with low holding current (<≈50 pA) and stable baseline were used. Input resistance (R_{in}), R_s, and membrane capacitance (C_m) were also measured before each recording by using 5 mV hyperpolarizing pulses. To ensure consistent recording qualities, only cells with $R_s < 20$ MΩ, $R_{in} > 500$MΩ, and $C_m > 10$ pF were accepted.

Spontaneous firing activity of GnRH-GFP neurons was recorded in whole-cell current clamp mode at 0 pA holding current. Measurements started with a control recording (1 min). Then a single bolus of neurotensin (500 nM; Tocris, Cat No 1909/1) (59) was pipetted into the measurement chamber filled with aCSF and the recording continued for another 7 min period.

A second set of experiments addressed to what extent the NTS2 receptor contributes to the action of neurotensin. The slices were first preincubated with the selective NTS2 receptor antagonist NTRC-824 (100 µM; Tocris, Cat. No. 5438/10) (60) for 9 min after the 1-min control period. Firing rates after the addition of NTRC-824 were used to determine whether the antagonist treatment itself has any effect on GnRH neuronal activity. The same neurons were recorded again in the presence of NTRC-824 to obtain a second 1-min control trace. Then a single bolus of neurotensin (500 nM) was added to the NTRC-824–containing aCSF for 7 min. Each neuron served as its own control while drug effects were evaluated.

Statistical analysis

Recordings were stored and analyzed offline. Event detection was performed using the Clampfit module of the pClamp 10.7 software (Molecular Devices Co).

Normality of all data in the statistical analysis was evaluated using the Shapiro–Wilk test. Mean firing rates were calculated as the number of action potentials divided by the control and treatment time periods, respectively. All the recordings were self-controlled in each neuron and the effects were expressed as percentages relative to the rates of the control periods.

Data availability

RNA-Seq files for $ChINs_{ZsG}$ neurons (called CPU300 transcriptome in the original publication) (10) are available in BioProject with the accession number PRJNA901862. New sequencing data have been deposited under PRJNA1131978 (Release date 1/31/2025).

Code availability

Scripts are available at https://github.com/goczbalazs/PRJNA1131978.

Supporting information—This article contains supporting information.

Ethics declaration—Animal experiments were carried out in accordance with the Institutional Ethical Codex, Hungarian Act of Animal Care and Experimentation (1998, XXVIII, section 243/1998) and the European Union guidelines (directive 2010/63/EU) and approved by the Animal Welfare Committee of the HUN-REN Institute of Experimental Medicine. All efforts were made to minimize potential pain or suffering and to reduce the number of animals used.

Acknowledgments—S. S.-T. and B. G. are awardees of the New National Excellence Programme of Hungary. We would like to thank Drs. SM. Moenter and C. Fekete for kindly providing the GnRH-GFP mice and the POMC antibodies, respectively.

Author contributions—B. G., E. R., S. S.-T., K. S., S. T., M. S., I. F., S. P., and E. H. methodology; B. G., E. R., S. S.-T., K. S., S. T., M. S., I. F., S. P., and E. H. investigation; B. G., E. R., S. S.-T., K. S., S. T., M. S., I. F., and E. H. conceptualization; E. R. and E. H. writing–original

draft; K. S. and E. H. funding acquisition; K. S. and E. H. supervision; E. R. and E. H. writing–review and editing.

Funding and additional information—This work was supported by grants to Project no. RRF-2.3.1-21-2022-00011, titled National Laboratory of Translational Neuroscience implemented with the support provided by the Recovery and Resilience Facility of the European Union within the framework of Programme Széchenyi Plan Plus, the National Research, Development and Innovation Office (K138137 to E. H. and PD134837 to K. S.), and the Hungarian Research Network (SA-104/2021) of Hungary. The work of S. S.-T. received support by the award of the National Academy of Scientist Education program.

Conflicts of interests—The authors declare that they have no conflicts of interest with the contents of this article.

Abbreviations—The abbreviations used are: aCSF, artificial cerebrospinal fluid; ChAT, choline acetyltransferase; ChIN, cholinergic interneuron; Cm, membrane capacitance; CPM, counts per million; CPU, caudate-putamen; ERα, alpha estrogen receptor; ERβ, beta estrogen receptor; FFPE, formalin-fixed paraffin-embedded; GABA, gamma-aminobutyric acid; GnRH, gonadotropin-releasing hormone; GPCR, G protein-coupled receptor; HH, hypogonadotropic hypogonadism; IHC, immunohistochemistry; KEGG, Kyoto Encyclopedia of Genes and Genomes; LCM, laser-capture microdissection; Ni-DAB, nickel-diaminobenzidine; NTS2, type-2 neurotensin receptor; OXB, orexin B; PACAP, pituitary adenylate cyclase-activating polypeptide; PEN, polyethylene naphthalate; PFA, paraformaldehyde; PVSA, polyvinyl sulfonate; POMC, proopiomelanocortin; RIN, RNA integrity number; R_{in}, input resistance; R_s, series resistance; TH, tyrosine hydroxylase; TPM, transcripts per million; VRC, ribonucleoside vanadyl complex.

References

1. Merchenthaler, I., Kovacs, G., Lavasz, G., and Setalo, G. (1980) The preoptico-infundibular LH-RH tract of the rat. *Brain Res.* **198**, 63–74
2. Herbison, A. E. (2016) Control of puberty onset and fertility by gonadotropin-releasing hormone neurons. *Nat. Rev. Endocrinol.* **12**, 452–466
3. Skynner, M. J., Sim, J. A., and Herbison, A. E. (1999) Detection of estrogen receptor alpha and beta messenger ribonucleic acids in adult gonadotropin-releasing hormone neurons. *Endocrinology* **140**, 5195–5201
4. Hrabovszky, E., Shughrue, P. J., Merchenthaler, I., Hajszan, T., Carpenter, C. D., Liposits, Z., *et al.* (2000) Detection of estrogen receptor-beta messenger ribonucleic acid and 125I-estrogen binding sites in luteinizing hormone-releasing hormone neurons of the rat brain. *Endocrinology* **141**, 3506–3509
5. Todman, M. G., Han, S. K., and Herbison, A. E. (2005) Profiling neurotransmitter receptor expression in mouse gonadotropin-releasing hormone neurons using green fluorescent protein-promoter transgenics and microarrays. *Neuroscience* **132**, 703–712
6. Vastagh, C., Csillag, V., Solymosi, N., Farkas, I., and Liposits, Z. (2020) Gonadal cycle-dependent expression of genes encoding peptide-, growth factor-, and orphan G-protein-coupled receptors in gonadotropin-releasing hormone neurons of mice. *Front. Mol. Neurosci.* **13**, 594119
7. Burger, L. L., Vanacker, C., Phumsatitpong, C., Wagenmaker, E. R., Wang, L., Olson, D. P., *et al.* (2018) Identification of genes enriched in GnRH neurons by translating ribosome affinity purification and RNAseq in mice. *Endocrinology* **159**, 1922–1940
8. Wang, C., Gong, B., Bushel, P. R., Thierry-Mieg, J., Thierry-Mieg, D., Xu, J., *et al.* (2014) The concordance between RNA-seq and microarray data depends on chemical treatment and transcript abundance. *Nat. Biotechnol.* **32**, 926–932
9. Mortazavi, A., Williams, B. A., McCue, K., Schaeffer, L., and Wold, B. (2008) Mapping and quantifying mammalian transcriptomes by RNA-Seq. *Nat. Methods* **5**, 621–628
10. Rumpler, E., Gocz, B., Skrapits, K., Sarvari, M., Takacs, S., Farkas, I., *et al.* (2023) Development of a versatile LCM-Seq method for spatial transcriptomics of fluorescently-tagged cholinergic neuron populations. *J. Biol. Chem.* , 105121. https://doi.org/10.1016/j.jbc.2023.105121
11. Watson, R. E., Jr., Wiegand, S. J., Clough, R. W., and Hoffman, G. E. (1986) Use of cryoprotectant to maintain long-term peptide immunoreactivity and tissue morphology. *Peptides* **7**, 155–159
12. Hrabovszky, E., Vrontakis, M. E., and Petersen, S. L. (1995) Triple-labeling method combining immunocytochemistry and in situ hybridization histochemistry: demonstration of overlap between Fos-immunoreactive and galanin mRNA-expressing subpopulations of luteinizing hormone-releasing hormone neurons in female rats. *J. Histochem. Cytochem.* **43**, 363–370
13. Hallick, R. B., Chelm, B. K., Gray, P. W., and Orozco, E. M., Jr. (1977) Use of aurintricarboxylic acid as an inhibitor of nucleases during nucleic acid isolation. *Nucleic Acids Res.* **4**, 3055–3064
14. Fellig, J., and Wiley, C. E. (1959) The inhibition of pancreatic ribonuclease by anionic polymers. *Arch. Biochem. Biophys.* **85**, 313–316
15. Hrabovszky, E., Molnar, C. S., Sipos, M. T., Vida, B., Ciofi, P., Borsay, B. A., *et al.* (2011) Sexual dimorphism of kisspeptin and neurokinin B immunoreactive neurons in the infundibular nucleus of aged men and women. *Front. Endocrinol. (Lausanne)* **2**, 80
16. Skrapits, K., Sarvari, M., Farkas, I., Gocz, B., Takacs, S., Rumpler, E., *et al.* (2021) The cryptic gonadotropin-releasing hormone neuronal system of human basal ganglia. *Elife* **10**. https://doi.org/10.7554/eLife.67714
17. Gocz, B., Rumpler, E., Sarvari, M., Skrapits, K., Takacs, S., Farkas, I., *et al.* (2022) Transcriptome profiling of kisspeptin neurons from the mouse arcuate nucleus reveals new mechanisms in estrogenic control of fertility. *Proc. Natl. Acad. Sci. U. S. A.* **119**, e2113749119
18. Gocz, B., Takacs, S., Skrapits, K., Rumpler, E., Solymosi, N., Poliska, S., *et al.* (2022) Estrogen differentially regulates transcriptional landscapes of preoptic and arcuate kisspeptin neuron populations. *Front. Endocrinol. (Lausanne)* **13**, 960769
19. Ameur, A., Zaghlool, A., Halvardson, J., Wetterbom, A., Gyllensten, U., Cavelier, L., *et al.* (2011) Total RNA sequencing reveals nascent transcription and widespread co-transcriptional splicing in the human brain. *Nat. Struct. Mol. Biol.* **18**, 1435–1440
20. Vieth, B., Parekh, S., Ziegenhain, C., Enard, W., and Hellmann, I. (2019) A systematic evaluation of single cell RNA-seq analysis pipelines. *Nat. Commun.* **10**, 4667
21. Svensson, V., Natarajan, K. N., Ly, L. H., Miragaia, R. J., Labalette, C., Macaulay, I. C., *et al.* (2017) Power analysis of single-cell RNA-sequencing experiments. *Nat. Methods* **14**, 381–387
22. Hrabovszky, E., Steinhauser, A., Barabas, K., Shughrue, P. J., Petersen, S. L., Merchenthaler, I., *et al.* (2001) Estrogen receptor-beta immunoreactivity in luteinizing hormone-releasing hormone neurons of the rat brain. *Endocrinology* **142**, 3261–3264. https://doi.org/10.1210/endo.142.7.8176
23. Herbison, A. E., and Pape, J. R. (2001) New evidence for estrogen receptors in gonadotropin-releasing hormone neurons. *Front. Neuroendocrinol* **22**, 292–308
24. Suter, K. J., Song, W. J., Sampson, T. L., Wuarin, J. P., Saunders, J. T., Dudek, F. E., *et al.* (2000) Genetic targeting of green fluorescent protein to gonadotropin-releasing hormone neurons: characterization of whole-cell electrophysiological properties and morphology. *Endocrinology* **141**, 412–419
25. Boehm, U., Bouloux, P. M., Dattani, M. T., de Roux, N., Dode, C., Dunkel, L., *et al.* (2015) Expert consensus document: European Consensus Statement on congenital hypogonadotropic hypogonadism–pathogenesis, diagnosis and treatment. *Nat. Rev. Endocrinol.* **11**, 547–564
26. Cieslik, M., Chugh, R., Wu, Y. M., Wu, M., Brennan, C., Lonigro, R., *et al.* (2015) The use of exome capture RNA-seq for highly degraded RNA with application to clinical cancer sequencing. *Genome Res.* **25**, 1372–1381

27. Groelz, D., Sobin, L., Branton, P., Compton, C., Wyrich, R., and Rainen, L. (2013) Non-formalin fixative *versus* formalin-fixed tissue: a comparison of histology and RNA quality. *Exp. Mol. Pathol.* **94**, 188–194
28. Brown, A. L., and Smith, D. W. (2009) Improved RNA preservation for immunolabeling and laser microdissection. *RNA* **15**, 2364–2374
29. Zhang, X., Hu, C., Huang, C., Wei, Y., Li, X., Hu, M., *et al.* (2022) Robust acquisition of spatial transcriptional programs in tissues with immunofluorescence-guided laser capture microdissection. *Front. Cell Dev. Biol.* **10**, 853188
30. Trogan, E., Choudhury, R. P., Dansky, H. M., Rong, J. X., Breslow, J. L., and Fisher, E. A. (2002) Laser capture microdissection analysis of gene expression in macrophages from atherosclerotic lesions of apolipoprotein E-deficient mice. *Proc. Natl. Acad. Sci. U. S. A.* **99**, 2234–2239
31. Yoshizawa, J. M., and Wong, D. T. (2013) Salivary microRNAs and oral cancer detection. *Methods Mol. Biol.* **936**, 313–324
32. Donohue, D. E., Gautam, A., Miller, S. A., Srinivasan, S., Abu-Amara, D., Campbell, R., *et al.* (2019) Gene expression profiling of whole blood: a comparative assessment of RNA-stabilizing collection methods. *PLoS One* **14**, e0223065
33. Hahn, N., Bens, M., Kempfer, M., Reissig, C., Schmidl, L., and Geis, C. (2023) Protecting RNA quality for spatial transcriptomics while improving immunofluorescent staining quality. *Front. Neurosci.* **17**, 1198154
34. Gray, J. C. (1974) The inhibition of ribonuclease activity and the isolation of polysomes from leaves of the French bean, Phaseolus vulgaris. *Arch. Biochem. Biophys.* **163**, 343–348
35. Berger, S. L., Hitchcock, M. J., Zoon, K. C., Birkenmeier, C. S., Friedman, R. M., and Chang, E. H. (1980) Characterization of interferon messenger RNA synthesis in Namalva cells. *J. Biol. Chem.* **255**, 2955–2961
36. [preprint] So, J., Strobel, O., Wann, J., Kim, K., Paul, A., Acri, D. J., *et al.* (2024) Robust single nucleus RNA sequencing reveals depot-specific cell population dynamics in adipose tissue remodeling during obesity. *bioRxiv*. https://doi.org/10.1101/2024.04.08.588525
37. Skidmore, A. F., and Beebee, T. J. (1989) Characterization and use of the potent ribonuclease inhibitor aurintricarboxylic acid for the isolation of RNA from animal tissues. *Biochem. J.* **263**, 73–80
38. Earl, C. C., Smith, M. T., Lease, R. A., and Bundy, B. C. (2018) Polyvinylsulfonic acid: a Low-cost RNase inhibitor for enhanced RNA preservation and cell-free protein translation. *Bioengineered* **9**, 90–97
39. Nichterwitz, S., Chen, G., Aguila Benitez, J., Yilmaz, M., Storvall, H., Cao, M., *et al.* (2016) Laser capture microscopy coupled with Smart-seq2 for precise spatial transcriptomic profiling. *Nat. Commun.* **7**, 12139
40. Martinek, J., Lin, J., Kim, K. I., Wang, V. G., Wu, T. C., Chiorazzi, M., *et al.* (2022) Transcriptional profiling of macrophages in situ in metastatic melanoma reveals localization-dependent phenotypes and function. *Cell Rep. Med.* **3**, 100621
41. Joseph, S. A., Piekut, D. T., and Knigge, K. M. (1981) Immunocytochemical localization of luteinizing hormone-releasing hormone (LHRH) in Vibratome-sectioned. *Brain J. Histochem. Cytochem.* **29**, 247–254
42. Parkash, J., Messina, A., Langlet, F., Cimino, I., Loyens, A., Mazur, D., *et al.* (2015) Semaphorin7A regulates neuroglial plasticity in the adult hypothalamic median eminence. *Nat. Commun.* **6**, 6385
43. Ciofi, P. (2000) Phenotypical segregation among female rat hypothalamic gonadotropin-releasing hormone neurons as revealed by the sexually dimorphic coexpression of cholecystokinin and neurotensin. *Neuroscience* **99**, 133–147
44. Shivers, B. D., Harlan, R. E., Morrell, J. I., and Pfaff, D. W. (1983) Absence of oestradiol concentration in cell nuclei of LHRH-immunoreactive neurones. *Nature* **304**, 345–347
45. Hamilton, K. J., Arao, Y., and Korach, K. S. (2014) Estrogen hormone physiology: reproductive findings from estrogen receptor mutant mice. *Reprod. Biol.* **14**, 3–8
46. Barraclough, C. A., and Haller, E. W. (1970) Positive and negative feedback effects of estrogen on pituitary LH synthesis and release in normal and androgen-sterilized rats. *Endocrinology* **86**, 542–551
47. Hrabovszky, E., and Petersen, S. L. (2002) Increased concentrations of radioisotopically-labeled complementary ribonucleic acid probe, dextran sulfate, and dithiothreitol in the hybridization buffer can improve results of in situ hybridization histochemistry. *J. Histochem. Cytochem.* **50**, 1389–1400
48. Petersen, S. L., Ottem, E. N., and Carpenter, C. D. (2003) Direct and indirect regulation of gonadotropin-releasing hormone neurons by estradiol. *Biol. Reprod.* **69**, 1771–1778
49. Paxinos, G., and Watson, C. (2013). In *The Rat Brain in Stereotaxic Coordinates*, Elsevier, San Diego, CA
50. Paxinos, G., Franklin, K. B. J., eds. (2013) *The Mouse Brain in Stereotaxic Coordinates*. ,Academic Press, San Diego, CA
51. Peterfi, Z., Farkas, E., Nagyunyomi-Senyi, K., Kadar, A., Otto, S., Horvath, A., *et al.* (2018) Role of TRH/UCN3 neurons of the perifornical area/bed nucleus of stria terminalis region in the regulation of the anorexigenic POMC neurons of the arcuate nucleus in male mice and rats. *Brain Struct. Funct.* **223**, 1329–1341
52. Skrapits, K., Kanti, V., Savanyu, Z., Maurnyi, C., Szenci, O., Horvath, A., *et al.* (2015) Lateral hypothalamic orexin and melanin-concentrating hormone neurons provide direct input to gonadotropin-releasing hormone neurons in the human. *Front Cell Neurosci* **9**, 348
53. Bolger, A. M., Lohse, M., and Usadel, B. (2014) Trimmomatic: a flexible trimmer for Illumina sequence data. *Bioinformatics* **30**, 2114–2120
54. Martin, M. (2011) Cutadapt removes adapter sequences from high-throughput sequencing reads. *EMBnet J.* https://doi.org/10.14806/ej.17.1.200
55. Dobin, A., Davis, C. A., Schlesinger, F., Drenkow, J., Zaleski, C., Jha, S., *et al.* (2013) STAR: ultrafast universal RNA-seq aligner. *Bioinformatics* **29**, 15–21
56. Liao, Y., Smyth, G. K., and Shi, W. (2014) featureCounts: an efficient general purpose program for assigning sequence reads to genomic features. *Bioinformatics* **30**, 923–930
57. Robinson, M. D., McCarthy, D. J., and Smyth, G. K. (2010) edgeR: a Bioconductor package for differential expression analysis of digital gene expression data. *Bioinformatics* **26**, 139–140
58. Farkas, I., Kallo, I., Deli, L., Vida, B., Hrabovszky, E., Fekete, C., *et al.* (2010) Retrograde endocannabinoid signaling reduces GABAergic synaptic transmission to gonadotropin-releasing hormone neurons. *Endocrinology* **151**, 5818–5829
59. Bose, P., Rompre, P. P., and Warren, R. A. (2015) Neurotensin enhances glutamatergic EPSCs in VTA neurons by acting on different neurotensin receptors. *Peptides* **73**, 43–50
60. Thomas, J. B., Giddings, A. M., Wiethe, R. W., Olepu, S., Warner, K. R., Sarret, P., *et al.* (2014) Identification of N-[(5-[(4-methylphenyl)sulfonyl] amino-3-(trifluoroacetyl)-1H-indol-1-yl)acetyl]-l-leucine (NTRC-824), a neurotensin-like nonpeptide compound selective for the neurotensin receptor type 2. *J. Med. Chem.* **57**, 7472–7477